An Empirical Model and an Inversion Technique for Radar Scattering from Bare Soil Surfaces

Yisok Oh, Kamal Sarabandi, *Member, IEEE*, and Fawwaz T. Ulaby, *Fellow, IEEE*

Abstract— **Polarimetric radar measurements were conducted for bare soil surfaces under a variety of roughness and moisture conditions at L-, C-, and X-band frequencies at incidence angles ranging from $10°$ to $70°$. Using a laser profiler and dielectric probes, a complete and accurate set of ground truth data were collected for each surface condition, from which accurate measurements were made of the rms height, correlation length, and dielectric constant. Based on knowledge of the scattering behavior in limiting cases and the experimental observations, an empirical model was developed for $\sigma^\circ_{hh}, \sigma^\circ_{vv}$, and σ°_{hv} in terms of ks (where $k = 2\pi/\lambda$ is the wave number and s is the rms height) and the relative dielectric constant of the soil surface. The model, which was found to yield very good agreement with the backscattering measurements of this study as well as with measurements reported in other investigations, was used to develop an inversion technique for predicting the rms height of the surface and its moisture content from multipolarized radar observations.**

I. Introduction

Investigation of the radar backscattering response of natural surfaces is an important problem in remote sensing because of its potential in retrieving the desired physical parameters of the surface, namely, its soil moisture content and surface roughness. Although the problem of electromagnetic wave scattering from random surfaces has been investigated for many years, because of its complexity theoretical solutions exist only for limiting cases. When the surface profile deviates only slightly from that of a smooth surface, perturbation solutions can be used. In the classic treatment of the small perturbation method (SPM) [1], [2] it is required that the rms height be much smaller than the wavelength and the rms slope be on the same order of magnitude as the wavenumber times the rms height. Recently, a perturbation method based on perturbation expansion of the phase of the surface field (PPM) was developed which extends the region of validity of SPM to higher values of the rms height s, provided the slope remains relatively small [3]. The other limiting case is when surface irregularities are large compared to the wavelength, which is equivalent to having a large radius of curvature at each point on the surface. In this limit, the Kirchhoff approximation (KA) is applicable [4], [5]. Various types of modifications and improvements to this model can be found in the literature. In these papers, the effects of shadowing and multiple scattering are discussed, which basically extend the region of validity of the KA solution, but by only a limited extent [6]. Combined solutions of KA and SPM, which are applicable for composite surfaces, have basically the same regions of validity as the individual models [7].

At microwave frequencies many natural surfaces do not fall into the validity regions of the theoretical models, and even when they do, the available models fail to provide results in good agreement with experimental observations. This assertion will be demonstrated by the results of the present study. The major goal of this investigation is to determine the dependence of the radar backscatter on the roughness parameters and soil moisture content of natural surfaces through extensive backscatter measurements for a variety of moisture and roughness conditions, over a wide range of incidence angles and frequencies. Once the dependence of the radar backscatter on these parameters has been established, an empirical model can be used to retrieve the surface roughness and soil moisture content from measured radar data.

The radar measurements reported in this study were obtained by a truck-mounted network-analyzer-based scatterometer (LCX POLARSCAT) [8]. The data were recorded in a fully polarimetric format at L-, C-, and X-band frequencies at incidence angles ranging from $10°$ to $70°$. An empirical model was formulated using the magnitudes of the measured data, and another data set was used to verify the model performance. Excellent qualitative and reasonable quantitative agreements were obtained. The polarimetric measurements included recordings of the phase statistics of the backscattered signal, but these will not be discussed in this paper as they are the subject of a separate report.

Manuscript received June 1, 1991; revised September 26, 1991. This work was supported by NASA under grant NAGW-2151.

The authors are with the Radiation Laboratory, Department of Electrical Engineering and Computer Science, the University of Michigan, Ann Arbor, MI 48109-2122.

IEEE Log Number 9105684.

II. Experimental Procedure

Fig. 1 shows a diagram of the scatterometer system and drawings of the laser profiler and dielectric probe. A brief description of each follows.

A. Scatterometer

The University of Michigan's LCX POLASCAT [8] was designed with the capability to measure the scattering matrix of point or distributed targets at L-, C- and X-band (with center frequencies at 1.25, 4.75, and 9.5 GHz, respectively). The scatterometer consists of an automatic vector network analyzer (HP 8753A), a computer unit, a disk drive for data storage, an amplifying and pulsing circuitry for hardware range gating, a relay actuator, and L-, C-, and X-band RF

TABLE I
POLARIMETRIC SCATTEROMETER (POLARSCAT) CHARACTERISTICS

	L	*C*	*X*
Center Frequency	1.50 GHz	4.75 GHz	9.50 GHz
Frequency Bandwidth	0.3 GHz	0.5 GHz	0.5 GHz
Antenna Type		Dual Polarized Pyramidal Horn	
Antenna Gain	22.1 dB	25.3 dB	29.5 dB
Antenna Beamwidth	12.0°	8.0°	5.4°
Far Field ($2d^2/\lambda$)	8.5 m	5.8 m	10.5 m
Platform Height	18 m	18 m	18 m
Cross-pol Isolation†	45 dB	45 dB	45 dB
Calibration Accuracy	±0.3 dB	±0.3 dB	±0.3 dB
Measurement Precision ($N > 100$)	±0.4 dB	±0.4 dB	±0.4 dB
Phase Accuracy†	±3°	±3°	±3°

†After polarimetric calibration using STCT [9].

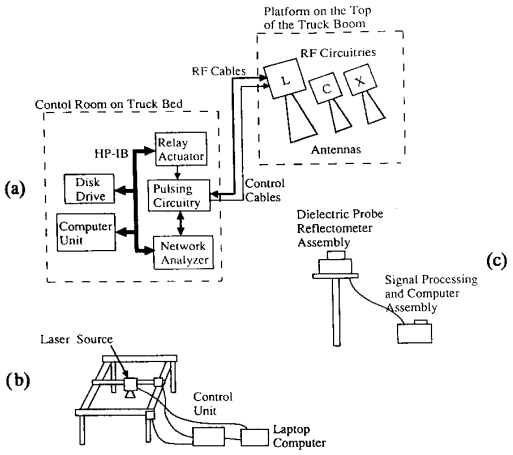

Fig. 1. Experimental system: (a) Scatterometer block diagram. (b) Laser profile meter. (c) Dielectric probe.

circuits and antennas, as shown in Fig. 1. The antennas are dual-polarized with orthogonal mode transducers (OMT) used for simultaneous transmission of a V-polarized signal and reception of both the V- and H- components of the backscattered signal. The process is then repeated for an H-polarized transmitted signal.

A computer is used to control the network analyzer (through an HP-IB interface bus) to acquire the desired data automatically. The computer also controls a relay actuator which energizes the desired frequency and polarization switches. Table I contains a list of the basic characteristics of the scatterometers, including specifications of the center frequencies, bandwidths, antenna characteristics, and overall performance.

To achieve good statistical representation of the measured backscatter for distributed targets, a large number of spatially independent samples are required. In this experiment 90 and 60 independent samples were taken at incidence angles of 10°, 20°, 30° and 40°, 50°, 60°, 70°, respectively. To achieve good range resolution, and also to increase the number of independent samples, the measurements were performed over bandwidths of 0.3 GHz for *L*-band and 0.5 GHz for *C*- and *X*-band. By treating the backscattering coefficient as constant over the mentioned bandwidths, the total number of independent samples represented by each measurement of the scattering coefficient σ°, including those achieved through frequency averaging, exceeds 1000 at most incidence angles.

In addition to the soil backscatter data, the noise background level was measured by pointing the antennas toward the sky. The noise background level was subtracted from the soil backscatter data coherently to improve the signal to noise ratio. The polarimetric response of a conducting sphere was measured to achieve absolute calibration of the radar system [9]. To minimize the time elapsed between the four polarization measurements comprising a single polarimetric data set, the soil backscatter data were collected in a raw-data format. The radar data was then postprocessed to separate the unwanted short-range returns from the target return using the time domain gating capability. The gated target response was then calibrated using the sphere data.

B. Laser Profile Meter

The height profiles of the soil surfaces were measured by a laser profile meter mounted on an *XY*-table, as shown in Fig. 1. The laser profiler, which is driven by a stepper motor, can measure a surface profile with 1 mm horizontal resolution and 2 mm vertical accuracy. A laptop computer is connected to the stepper-motor controllers to position the laser distance meter with the desired steps in the *X* and *Y* directions. The heights measured by the laser profiler are also collected and stored by the same computer. A minimum of ten 1-m profiles were collected for each surface with steps of 0.25 cm in the horizontal direction. In addition to the surface profiles acquired by the laser profiler, two 3-m profiles were collected using chart paper and spray paint to monitor large scale roughness variations. The radar measurements were conducted for four surface-roughness conditions, covering the range from 0.32 cm to 3.02 cm in rms height (Table II).

C. Dielectric Probe

The dielectric constant of the soil surface was measured by a *C*-band field-portable dielectric probe [10]. The probe consists of a reflectometer assembly with a coaxial probe tip and a signal processing assembly with a calculator. The dielectric

TABLE II
SUMMARY OF ROUGHNESS PARAMETERS

Surface	s (cm)	l (cm)	m	Freq(GHz)	ks	kl	
				1.50	0.13	2.6	L1
S-1	0.40	8.4	0.048†	4.75	0.40	8.4	C1
				9.50	0.80	16.7	X1
				1.50	0.10	3.1	L2
S-2	0.32	9.9	0.032†	4.75	0.32	9.8	C2
				9.50	0.64	19.7	X2
				1.50	0.35	2.6	L3
S-3	1.12	8.4	0.133†	4.75	1.11	8.4	C3
				9.50	2.23	16.7	X3
				1.50	0.95	2.8	L4
S-4	3.02	8.8	0.485‡	4.75	3.00	8.8	C4
				9.50	6.01	17.5	X4

s = rms height
ℓ = correlation length
m = rms slope
$k = 2\pi/\lambda$
†$m = s/l$ assuming exponential autocorrelation function
‡$m = \sqrt{2}s/l$ assuming Gaussian autocorrelation function

TABLE III
SUMMARY OF SOIL MOISTURE AND DIELECTRIC DATA

Surface Number	Measured ϵ_r (4.8 GHz)		Estimated m_v		calculated (ϵ_r, ϵ_r) for (0-4 cm) layer		
	Top Soil	4 cm depth	Top	4 cm	1.5 GHz	4.75 GHz	9.5 GHz
1 -wet	14.15	16.74	0.29	0.33	15.57, 3.71	15.42, 2.15	12.31, 3.55
1 -dry	6.58	11.05	0.14	0.24	7.99, 2.02	8.77, 1.04	5.70, 1.32
2 -wet	14.66	14.30	0.30	0.29	14.43, 3.47	14.47, 1.99	12.64, 3.69
2 -dry	4.87	8.50	0.09	0.19	5.85, 1.46	6.66, 0.68	4.26, 0.76
3 -wet	15.20	15.10	0.31	0.31	15.34, 3.66	15.23, 2.12	13.14, 3.85
3 -dry	7.04	10.02	0.15	0.22	7.70, 1.95	8.50, 1.00	6.07, 1.46
4 -wet	8.80	10.57	0.19	0.23	8.92, 2.24	9.64, 1.19	7.57, 1.99
4 -dry	7.28	8.84	0.16	0.19	7.23, 1.83	8.04, 0.92	6.28, 1.53

constant was measured at the soil surface and at a depth of 4 cm at each of more than 50 locations randomly chosen over each surface. The relative dielectric constant (ϵ_r) was used to estimate the moisture contents (m_v) by inverting a semiempirical model [11] which gives ϵ_r in terms of m_v. The real part of ϵ_r was used in the dielectric-to-moisture inversion because the error in measuring the imaginary part of ϵ_r by the dielectric probe is relatively higher [12]. The mean value of m_v was then used in the same semiempirical model to obtain an estimate for ϵ_r at L-, C-, and X-band. Table III gives the measured values of ϵ_r' at 4.8 GHz and the estimated values of m_v for the top surface and 4-cm deep layers, from which the 0–4 cm average dielectric constant was calculated at L-, C-, and X-band. Soil density was determined from soil samples with known volume.

III. EXPERIMENTAL OBSERVATIONS AND COMPARISON WITH CLASSICAL SOLUTIONS

In this section we present samples of the measured radar data to illustrate the spectral, angular, and polarization behavior of rough surface scattering. Next, for surfaces whose statistical roughness parameters fall within the region of validity of theoretical models, we will compare the experimental observations with theoretical predictions.

A. Experimental Observations

Four different fields (S1, S2, S3, and S4) were examined in this study. Each was measured under two different moisture conditions, relatively wet and relatively dry. The roughness parameters of the surfaces, such as the rms height s, autocorrelation function $\rho(\xi)$, correlation length l, and rms slope m, were calculated from the measured surface height profiles and are given in Table II.

Based on an analysis of the surface-height distributions, we concluded that the surface-height deviation is approximately Gaussian for all four surfaces, with a probability density function given by

$$p(z) = \frac{1}{\sqrt{2\pi}s} \exp\left[-\frac{z^2}{2s^2}\right]. \quad (1)$$

For the first three surfaces, the measured autocorrelation function $\rho(\xi)$ was found to be closer in shape to an exponential function of the form

$$\rho(\xi) = \exp[-|\xi|/\ell] \quad (2)$$

than to the Gaussian function

$$\rho(\xi) = \exp[-\xi^2/\ell^2]. \quad (3)$$

The Gaussian form provided a better fit for the roughest field, S4. This is illustrated in Fig. 2 for fields S1 and S4. The

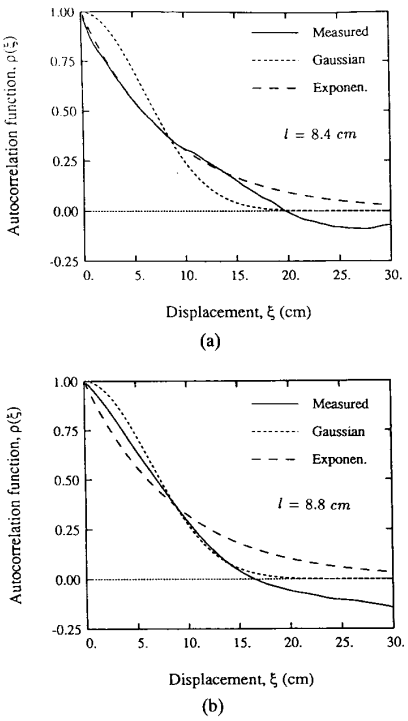

Fig. 2. Comparison of the measured autocorrelation functions with the Gaussian and exponential functions for surfaces (a) S1 and (b) S4.

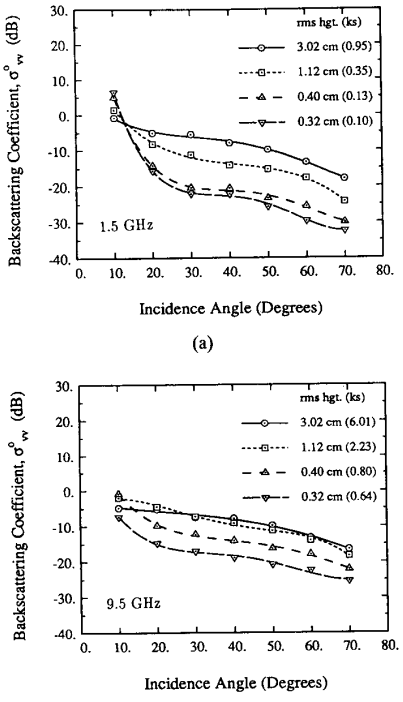

Fig. 3. Angular response of σ°_{vv} for four different surface roughnesses at moderately dry moisture condition ($m_v \simeq 0.15$) at (a) 1.5 GHz and (b) 9.5 GHz.

surface rms slope can be calculated from $m = s\sqrt{\mid \rho''(0) \mid}$, where $\rho''(0)$ is the second derivative of $\rho(\xi)$ evaluated at $\xi = 0$, which yields $m = s/l$ for the exponential function and $m = \sqrt{2}s/l$ for the Gaussian function.

Among the four surfaces, surface S2 is the smoothest ($s = 0.32$ cm), surface S1 ($s = 0.4$ cm) is slightly rougher, surface S3 ($s = 1.12$ cm) represents an intermediate-roughness condition, and surface S4 ($s = 3.02$ cm) is a very rough surface that was generated by ploughing the top 15-cm surface layer. Electromagnetically, these surfaces cover a wide range of roughness conditions (Table II), extending from $ks = 0.1$ to $ks = 6.01$ (where $k = 2\pi/\lambda$ is the wave number) and from $k\ell = 2.6$ to $k\ell = 19.7$. The 12 roughness conditions corresponding to the four surfaces and three wavelengths are identified in $ks - k\ell$ space in Fig. 7, together with the boundaries for the regions of validity of the small perturbation model (SPM) and the physical optics (PO) and geometric optics (GO) solutions of the Kirchhoff approximation.

Fig. 3 shows angular responses of the vv-polarized backscattering coefficient (σ°_{vv}) for four different bare soil surfaces with rms heights ranging from 0.3 cm to 3.0 cm, all at a moderately dry moisture condition ($m_v \simeq 0.15$). The sensitivity of σ°_{vv} to surface roughness is clearly evident at both 1.5 GHz (Fig. 3(a)) and 9.5 GHz (Fig. 3(b)); over the $30° - 70°$ angular range, σ°_{vv} exhibits a dynamic range of 16 dB at 1.5 GHz and 10 dB at 9.5 GHz, corresponding to the surface roughness (s) range from 0.3 cm to 3 cm. We also observe that at 9.5 GHz, the surfaces with $ks = 2.23$ and 6.01 exhibit approximately the same radar response, suggesting that σ°_{vv} becomes approximately insensitive to surface roughness for $ks \geq 2.0$.

Further illustration of the effect of surface roughness on the angular response of σ° is shown in Fig. 4, which contains plots of the three principal polarization components for the smoothest case (Fig. 4(a)), corresponding to surface S2 at 1.5 GHz, and for the roughest-surface condition (Fig. 4(b)), corresponding to surface S4 at 9.5 GHz. Based on these and on the data measured for the other surfaces, we note that the ratio of σ°_{hh} to σ°_{vv}, which will be referred to as the copolarized ratio, is always smaller than or equal to 1, and it approaches 1 as ks becomes large. Very rough surfaces, such as C4 (surface 4 at C-band) and X4, do not show any noticeable differences between σ°_{vv} and σ°_{hh}, while smooth surfaces show values of $\sigma^\circ_{hh}/\sigma^\circ_{vv}$ smaller than 1. It is also observed that the copolarized ratio is a function of incidence angle for smooth surfaces and decrease as the incidence angle increases. The sensitivity of the copolarized ratio ($\sigma^\circ_{hh}/\sigma^\circ_{vv}$) to surface roughness and incidence angle is shown in Fig. 5. For very rough surfaces ($ks \geq 3$), $\sigma^\circ_{hh}/\sigma^\circ_{vv} \simeq 1$ and is independent of incidence angle. Another point worth noting is that the shape of the angular pattern of the cross-polarized backscattering coefficient σ°_{hv}, is similar to that of σ°_{vv}, but the ratio $\sigma^\circ_{hv}/\sigma^\circ_{vv}$, which will be referred to as the cross-polarized ratio, increases with ks as shown in Figs. 4(a) and (b) (and more explicitly in Fig. 11).

The backscattering coefficient of a surface is also a function of its moisture content. Fig. 6(a) shows the backscattering

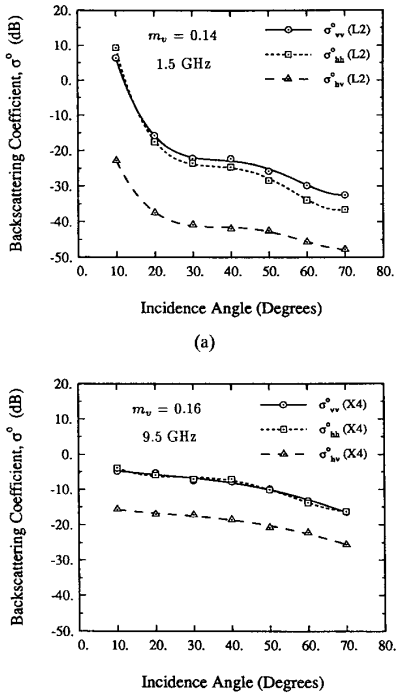

Fig. 4. Angular responses of $\sigma^\circ_{vv}, \sigma^\circ_{hh}$ and σ°_{hv} for (a) a smooth surface at 1.5 GHz (L2) and (b) a very rough surface at 9.5 GHz (X4).

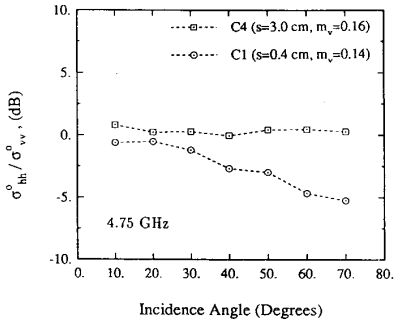

Fig. 5. Angular dependence of the copolarized ratio, $\sigma^\circ_{hh}/\sigma^\circ_{vv}$, at 4.75 GHz for a smooth surface and a very rough surface.

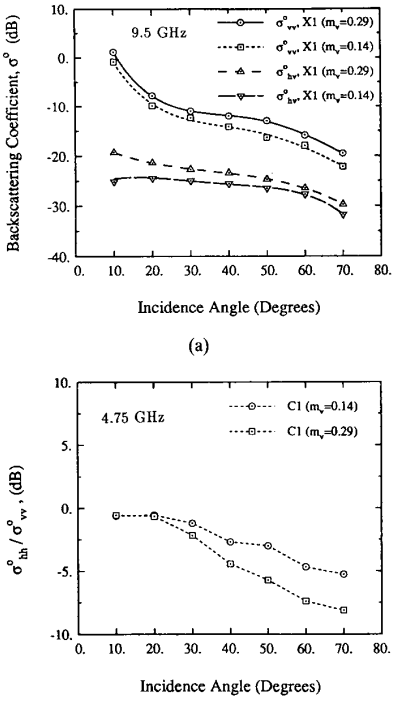

Fig. 6. Angular plots of (a) σ°_{vv} and σ°_{hv} of surface S1 at X-band for two different moisture conditions and (b) the copolarized ratio, $\sigma^\circ_{hh}/\sigma^\circ_{vv}$, for the same surface at C-band.

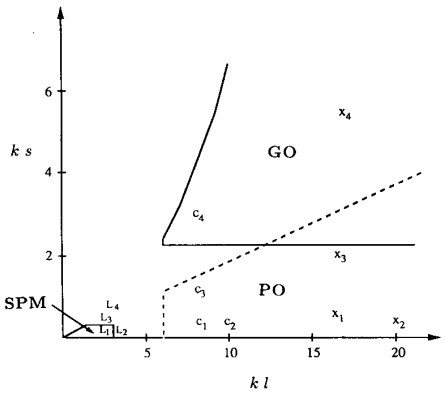

Fig. 7. Roughness parameters and the region of validity of SPM, PO, and GO models.

coefficient of surface 1 for two moisture conditions, $m_v = 0.29$ and $m_v = 0.14$. The ratio of σ°_{vv} (or σ°_{hv}) of wet soil to σ°_{vv} (or σ°_{hv}) of dry soil is about 3 dB at incidence angles in the 20° to 70° range. Fig. 6(b) shows the angular response of the copolarized ratio $\sigma^\circ_{hh}/\sigma^\circ_{vv}$ for a fixed roughness at two different moisture contents. The magnitude of the copolarized ratio is larger for the wet surface (6 dB at 50°) than for the dry surface (3 dB at 50°).

B. Comparison with Classical Solution

This section evaluates the applicability of the small perturbation method (SPM), the physical optics (PO) model, and the geometric optics (GO) model to the measured radar data. Expressions for the backscattering coefficient σ° and the regions of validity of these models are given in [5]. The locations of the 12 surface roughness conditions are identified in $ks - kl$ space in Fig. 7. Also shown are the regions of validity of the SPM, PO, and GO models for random surfaces characterized by a Gaussian autocorrelation function. The lower limit of the ks value of the validity region of the GO model is given by $ks > \sqrt{2.5}/\cos\theta$, which varies from 1.62 at 10° to 6.32 at 60°. The limit shown in Fig. 7 corresponds to $\theta = 40°$.

TABLE IV
AUTOCORRELATION FUNCTIONS AND THE CORRESPONDING ROUGHNESS SPECTRA

Normalized $\rho(\xi)$	$W(2k \sin\theta)$
Gaussian: $\exp[-\xi^2/l^2]$	$(l^2/2)\cdot\exp[-(kl\sin\theta)^2]$
Exponential: $\exp[-\lvert\xi\rvert/l]$	$(l^2/2)\cdot[1+(2kl\sin\theta)^2]^{-1}$
Measured: Numerical data	Fourier Transform of $\rho(\xi)$

According to Fig. 7, some of the surface roughness conditions fall outside the regions of validity of all three models, while several satisfy the model conditions. In order to compare the measured data with model predictions, we have selected surface 1 at 1.5 GHz (L1) to compare with the SPM, surface 1 at 9.5 GHz (X1) to compare with the PO model, and surface 4 at 9.5 GHz (X4) to compare with the GO model.

1) Small Perturbation Model: The measured angular responses of σ°_{vv} and σ°_{hh} are shown in Figs. 8(a) and (b) for data set L1 (surface 1 at 1.5 GHz), together with plots calculated using the SPM for each of three autocorrelation functions: a Gaussian function of the form given by (3), an exponential function of the form given by (2), and the measured autocorrelation function obtained from the measured surface profile, which is approximately exponential in form (Fig. 2(a)). The calculated curves include a coherent component to account for the strong backscatter response near normal incidence (see Table IV).

Overall, SPM provides a reasonable fit for σ°_{hh} when used in conjunction with the exponential correlation function, but not as well for σ°_{vv}. Fig. 8(c) provides a comparison of the measured data for $\sigma^\circ_{vv}, \sigma^\circ_{hh}$, and σ°_{hv} with SPM calculated using the exponential correlation function. The cross-polarized backscattering coefficient σ°_{hv}, which was computed using the second-order SPM [2], is in close agreement with data and exhibits an angular response similar to that of σ°_{vv} (at angles greater than 20°).

2) Physical Optics Model: Several of the surface roughness conditions examined in this study fall within the region of validity of the PO model. We have chosen X1 for detailed examination in this section. The plots shown in Fig. 9 indicate that the PO model provides good agreement with measured data for σ°_{hh} when an exponential correlation function is used, but the model underestimates σ°_{vv} at angles beyond 40° . Since the PO approximation does not account for cross-polarization in the backscattering direction, comparison with the measured σ°_{hv} data is not warranted.

Similar comparisons between theory and measured data were performed for the other five surface conditions that, according to Fig. 7, satisfy the validity conditions of the PO model. In all cases, the deviation between theory and measurements was greater than what was noted above for X1 (Fig. 9), with some of the deviations being as large as 20 dB. Furthermore, the level of the measured angular response of σ°_{vv} was observed to be always greater or equal to that of σ°_{hh} for all surfaces, moisture contents, and incidence angles, which is contrary to the behavior of the PO model.

3) Geometrical Optics Model: For angles below 50°, the GO model was found to differ from the measured angular responses of σ°_{hh} and σ°_{vv} by 3 dB or less for surface condition X4 (Fig. 10) and by 4 dB or less for C4. The coherent component of the backscattering coefficient is negligibly small for a very rough surface, and the noncoherent component dominates at all angles including normal incidence.

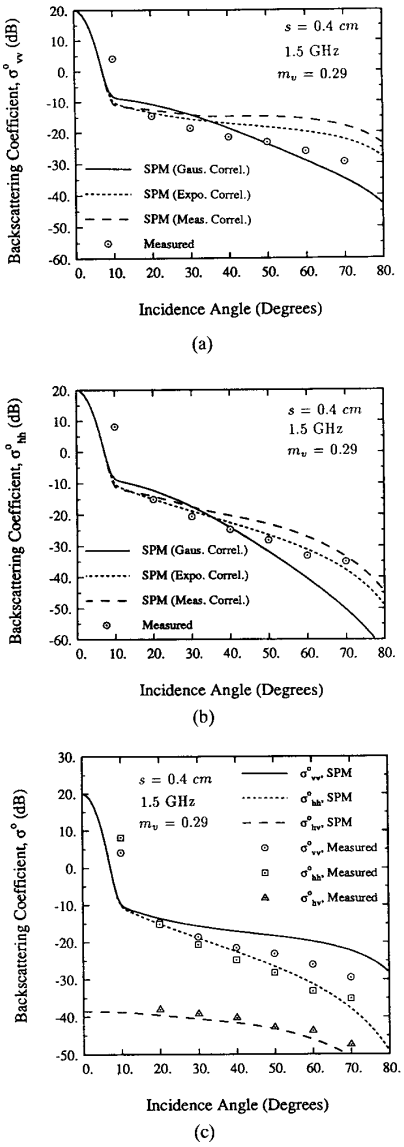

Fig. 8. SPM model with different autocorrelation functions compared to the measured data of L1 (surface 1 at 1.5 GHz, ks=0.13) for (a) VV-polarization, (b) HH-polarization, and for (c) VV-, HH-, and HV-polarizations using an exponential autocorrelation function.

The major conclusions we drew from our analysis of the measured radar data when compared with the predictions of the SPM, PO, and GO models are:

1) Some natural surface conditions fall outside the regions of validity of all three models.
2) None of the models provides consistently good agreement with the measured data, particularly at incidence angles greater than 40°.

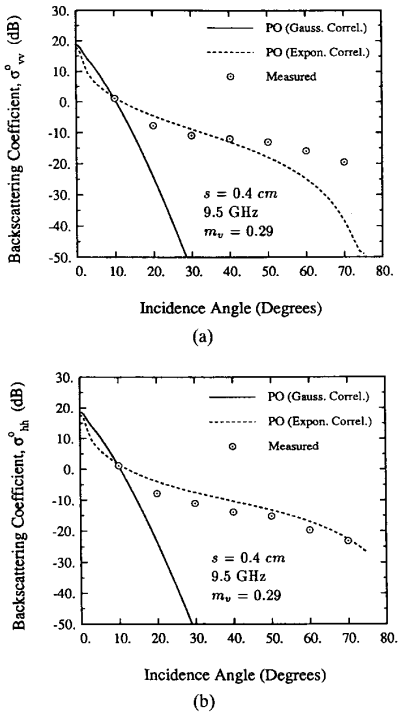

Fig. 9. PO model with different autocorrelation functions compared to the measured data of X1 (surface 1 at 9.5 GHz, ks=0.80) for (a) VV-polarization, and (b) HH-polarization.

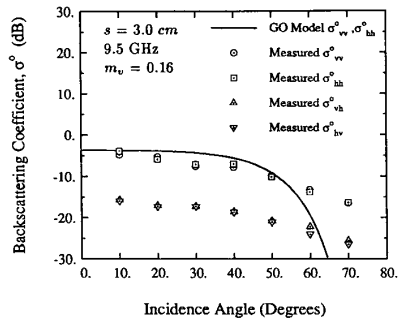

Fig. 10. GO model compared to the measured data of X4 (surface 4 at 9.5 GHz, ks=6.0).

3) The PO model predicts that $\sigma^\circ_{vv} < \sigma^\circ_{hh}$, contrary to all observations.

In addition, since they are first-order solutions, both the PO and GO models cannot be used for σ°_{hv}. Faced with these inadequacies of the available theoretical scattering models, we decided to develop an empirical model that relates $\sigma^\circ_{vv}, \sigma^\circ_{hh}$, and σ°_{hv} to the roughness (ks) and dielectric constant (ϵ_r) of the surface. This is the subject of the next section.

IV. Empirical Model

The empirical model developed in this section is based on the radar backscatter data measured in this investigation and on knowledge of the scattering behavior in the limiting

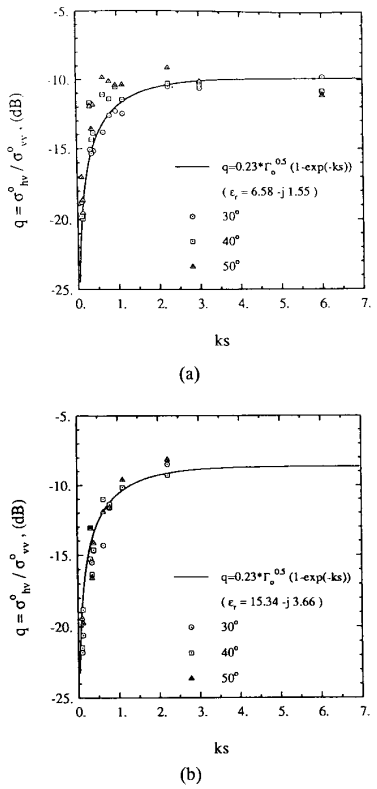

Fig. 11. The sensitivity of the cross-polarized ratio, $\sigma^\circ_{hv}/\sigma^\circ_{vv}$, to surface roughness for (a) dry soil and (b) wet soil.

cases (such as when ks is very large). For this data set, the surface roughness and moisture content cover the ranges: $0.1 < ks < 6.0, 2.6 < k\ell < 19.7$, and $0.09 < m_v < 0.31$.

We begin with an examination of the cross-polarized ratio $q = \sigma^\circ_{hv}/\sigma^\circ_{vv}$. We observed from the measured angular responses that σ°_{hv} and σ°_{vv} exhibit similar variations with incidence angle, particularly over the $30° - 50°$ range, for all surface roughnesses, moisture contents, and frequencies. Figs. 11(a) and (b) show the measured values of q as a function of ks for dry and wet soils, respectively. They include the values measured at $30°, 40°$, and $50°$ for all surface-frequency combinations. We observe that for the dry soils q increases rapidly from about -20 dB at $ks = 0.1$ to about -10 dB at $ks = 3$, and then maintains that level for $ks > 3$. For the wet soils, q exhibits a similar behavior as that noted for the dry soils, except that its saturation level is closer to -8.5 dB for $ks > 3$.

The curves shown in Fig. 11, which provide a good fit to the data, are given by the empirically determined function

$$q \triangleq \frac{\sigma^\circ_{hv}}{\sigma^\circ_{vv}} = 0.23\sqrt{\Gamma_\circ}[1 - \exp(-ks)] \tag{4}$$

where $\Gamma_\circ$ is the Fresnel reflectivity of the surface at nadir,

$$\Gamma_\circ = \left|\frac{1-\sqrt{\epsilon_r}}{1+\sqrt{\epsilon_r}}\right|^2. \tag{5}$$

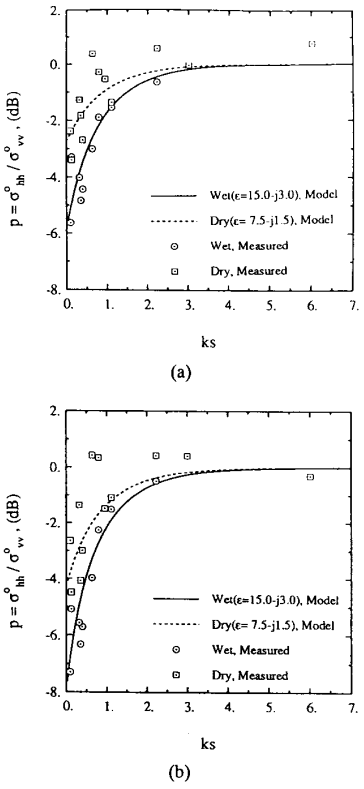

Fig. 12. The sensitivity of the copolarized ratio, $\sigma^\circ_{hh}/\sigma^\circ_{vv}$, to surface roughness and soil moisture, at (a) 40°, and (b) 50°.

Next, we shall examine the copolarized ratio $p = \sigma^\circ_{hh}/\sigma^\circ_{vv}$. The measured values of this ratio are shown in Fig. 12 for wet and dry moisture conditions at 40° and 50°. For very smooth surfaces, this ratio is about −6 dB, and for very rough surfaces it is equal to 0 dB. Similar results were obtained at 30°. The curves shown in Fig. 12 are based on the empirical expression

$$\sqrt{p} \triangleq \sqrt{\frac{\sigma^\circ_{hh}}{\sigma^\circ_{vv}}} = 1 - \left(\frac{2\theta}{\pi}\right)^{[1/3\Gamma_\circ]} \cdot \exp(-ks) \qquad (6)$$

where θ is the incidence angle in radians.

Having established empirical formulas for $q = \sigma^\circ_{hv}/\sigma^\circ_{vv}$ and $p = \sigma^\circ_{hh}/\sigma^\circ_{vv}$ that provide reasonable agreement with the measured data, the remaining task is to relate the absolute level of any one of the three linearly polarized backscattering coefficients to the surface parameters. Upon examining the measured data, we developed the following empirical expression for the magnitude of σ°_{vv}:

$$\sigma^\circ_{vv}(\theta, \epsilon_r, ks) = \frac{g\cos^3\theta}{\sqrt{p}} \cdot [\Gamma_v(\theta) + \Gamma_h(\theta)] \qquad (7)$$

where

$$g = 0.7\Big[1 - \exp\Big(-0.65(ks)^{1.8}\Big)\Big] \qquad (8)$$

and p is as given by (6).

With the ratios p and q being given explicitly in terms of ks and ϵ_r (through $\Gamma_\circ$) and the function g being governed by only ks, the three linearly polarized backscattering coefficients are given by (7) for σ°_{vv} and by

$$\sigma^\circ_{hh}(\theta, \epsilon_r, ks) = g\sqrt{p}\cos^3\theta[\Gamma_v(\theta) + \Gamma_h(\theta)] \qquad (9)$$

and

$$\sigma^\circ_{hv}(\theta, \epsilon_r, ks) = q\sigma^\circ_{vv}(\theta, \epsilon_r, ks). \qquad (10)$$

for the other two components. We note that both σ°_{vv} and σ°_{hh} are proportional to the average of the vertically and horizontally polarized Fresnel reflectivities of the surface at the incidence angle θ. The HH component is smaller than the VV component by a multiplying factor $p(p \leq 1)$. For $ks > 3, p \simeq 1$ and $\sigma^\circ_{vv} \simeq \sigma^\circ_{hh}$. For smaller values of ks, the factor p accounts for the difference in level between σ°_{vv} and σ°_{hh} and includes a dependence on ϵ_r.

Aside from the dependence on θ inherent in the quantity $[\Gamma_v(\theta) + \Gamma_h(\theta)]$ and in the function p, both σ°_{vv} and σ°_{hh} vary as $\cos^3\theta$. A more elaborate functional dependence for the power of $\cos\theta$ can be devised in terms of ϵ_r and ks, but this was found to be unnecessary. As we will see next, the empirical model was found to provide a good representation of the measured data at all frequencies and over a wide angular range. The model was evaluated against three data sets: (a) the data measured in this study, (b) another independently measured data set that was not used in the development of the model, which shall be refered to as Independent Data Set II, and (c) a data set that was recently reported by Yamasaki *et al.* [13] at 60 GHz.

A. Comparison With Measured Data

Because of space limitations, we will present only two typical examples illustrating the behavior of the empirical model, in comparison with the data measured in this study. This is shown in Figs. 13 and 14 for surface S1 (representing a very smooth surface with $s = 0.40$) and surface S4 (representing a very rough surface with $s = 3.02$). In both cases, very good agreement is observed between the model and the measured data at all three frequencies and across the entire angular range between 20° and 70°. The levels of the measured values of σ°_{vv} and σ°_{hh} at $\theta = 10°$ for surface S1 include a strong contribution due to the coherent backscattering component that exists at angles close to normal incidence. No attempt has been made at this stage to add a coherent component to the empirical model, and, therefore, its range of applicability does not include the angular range below 20° for smooth surfaces. If the surface is rough, as is the case for surface S4 (Fig. 14), the coherent backscattering coefficient is negligibly small, in which case the empirical model may be used at all angles between 0° and 70°.

B. Comparison With Independent Data Set II

Prior to conducting the measurements reported in this study, another data set was acquired by the same radar system for three surface roughnesses. The surface profiles were measured by inserting a plate into the surface and spraying it with paint. Such a technique provides an approximate representation of the surface, but it is not as accurate as that obtained using

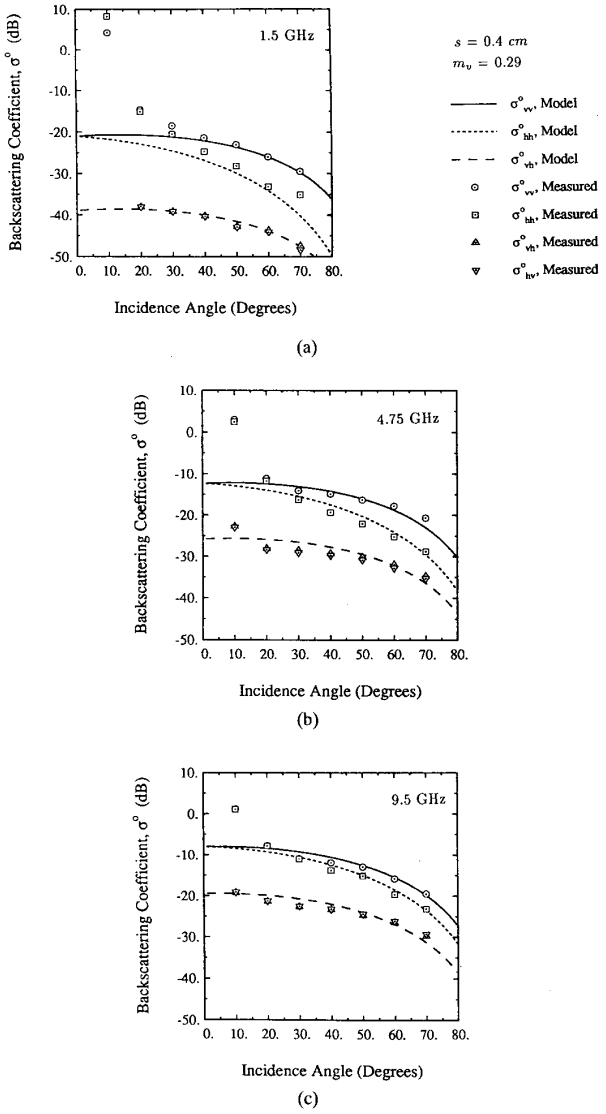

Fig. 13. Empirical model compared to the measured data of surface 1 for wet soil at (a) 1.5 GHz, (b) 4.75 GHz, and (c) 9.5 GHz.

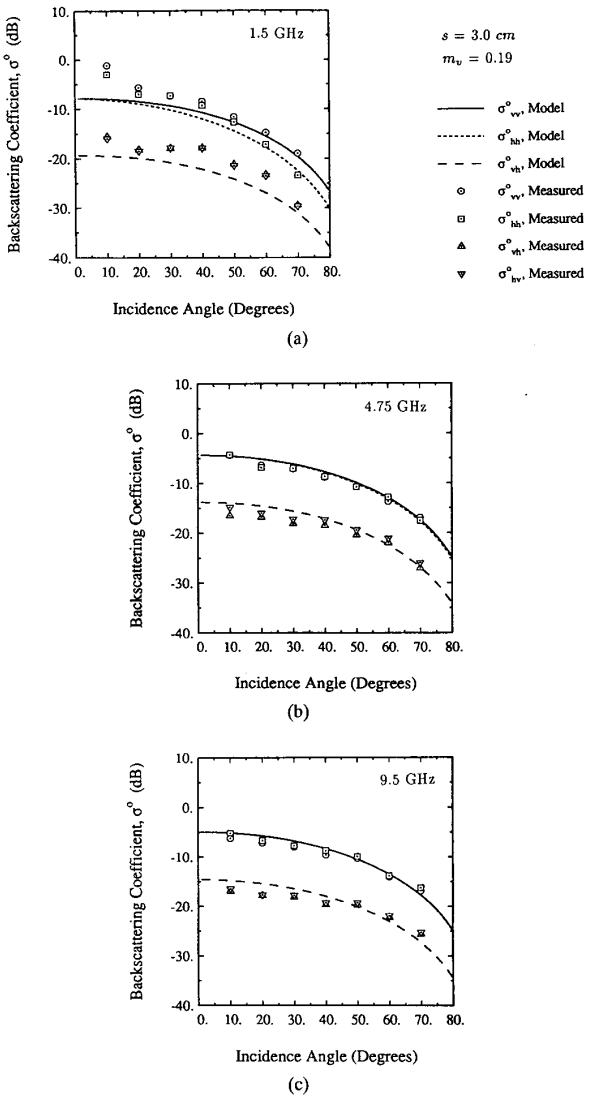

Fig. 14. Empirical model compared to the measured data of surface 4 for wet soil at (a) 1.5 GHz, (b) 4.75 GHz, and (c) 9.5 GHz.

the laser profiler. Hence, our estimate of the values of ks and kl for Independent Data Set II are not as accurate as those we obtained with the laser profiler for the surfaces discussed in the preceding sections of this paper. Nevertheless, we conducted an evaluation of the empirial model by comparing its prediction with the backscatter data of Independent Data Set II and found the agreement to be very good at all three frequencies, provided we are allowed to modify the value of s measured with the metal plate technique. An example is given in Fig. 15 in which the curves were calculated using the empirical model with $s = 0.7$ cm; the value of s estimated from the metal-plate record was 0.46 cm.

C. Comparison With 60 GHz Data

Our final comparison is with a 60 GHz data set that was recently reported by Yamasaki *et al.* [13]. Even though $k = 2\pi/\lambda = 1260$ at 60 GHz, the three surfaces examined in this study were extremely smooth, with rms heights of 0.055, 0.12, and 0.20 cm. The corresponding values of ks are 0.16, 0.64, and 1.75. Good overall agreement is observed (Fig. 16) between this data and the empirical model, despite the fact that the correlation lengths for all three surfaces are smaller than the smallest correlation length of the surfaces on the basis of which the empirical model was developed.

V. Inversion Model

Having established in the preceding section that the empirical model is a good estimator of $\sigma^\circ_{vv}, \sigma^\circ_{hh}$, and σ°_{hv} over a wide range of ks (0.1 to 6), we shall now invert the model to obtain estimates of s and the moisture content m_v from

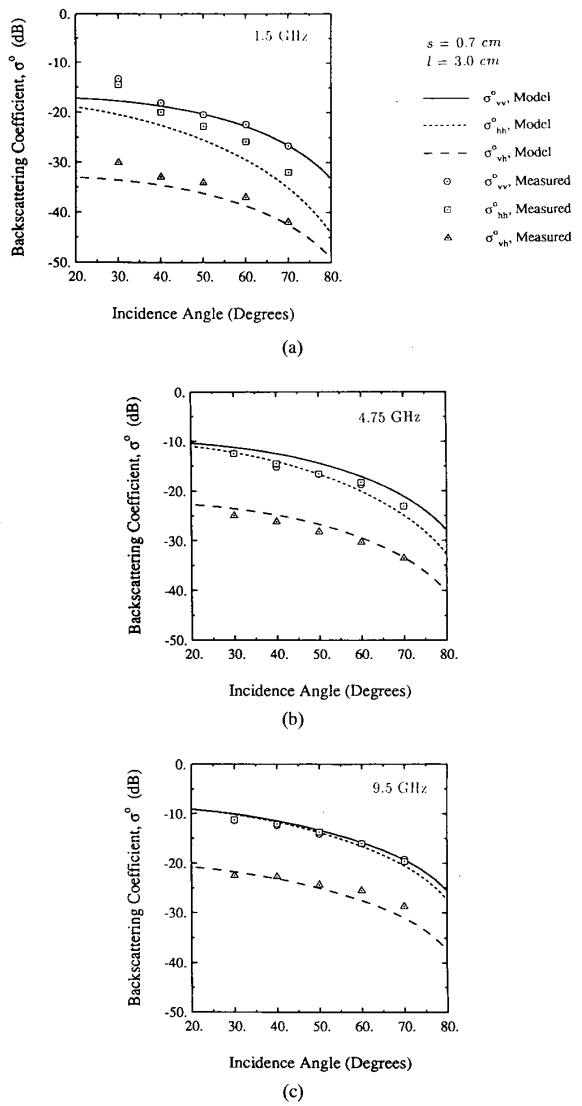

Fig. 15. Empirical model compared with the data from independent data set II for a surface with $s = 0.7$ cm and $l = 3.0$ cm, measured at (a) 1.5 GHz, (b) 4.75 GHz, and (c) 9.5 GHz.

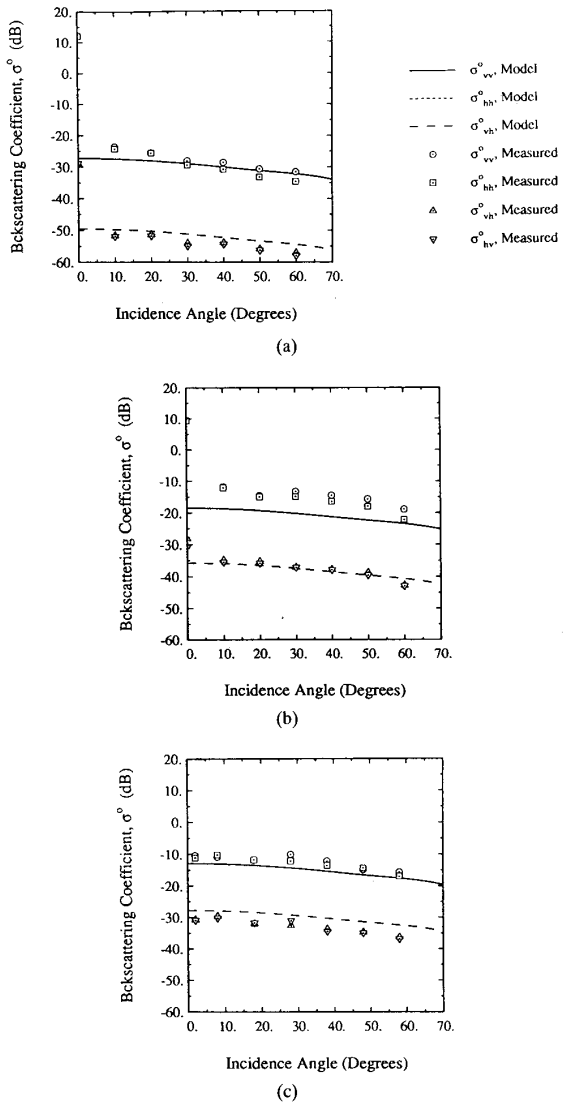

Fig. 16. Empirical model compared with the data reported by Yamasaki *et al.* [13] at 60 GHz for (a) soil-1 ($s = 0.013$ cm, $\ell = 0.055$ cm), (b) soil-2 ($s = 0.051$ cm, $\ell = 0.12$ cm), and (c) for soil-3 (s=2.88 cm, l=0.20 cm).

observation of $\sigma^\circ_{vv}, \sigma^\circ_{hh}$, and σ°_{hv}. Because the empirical model was developed on the basis of data for surfaces with kl in the range $2.6 < kl < 19.7$, we cannot ascertain its applicability or the applicability of the inversion model for surfaces with kl outside this range.

Suppose we have measurements of $\sigma^\circ_{vv}, \sigma^\circ_{hh}$, and σ°_{hv} for a given surface at a given incidence angle θ and wavelength λ. From these measurements, we compute the copolarized and cross-polarized ratios $p = \sigma^\circ_{hh}/\sigma^\circ_{vv}$ and $q = \sigma^\circ_{hv}/\sigma^\circ_{vv}$. By eliminating ks from (4) and (6), we obtain the following nonlinear equation for $\Gamma_\circ$:

$$\left(\frac{2\theta}{\pi}\right)^{1/3\Gamma_\circ} \cdot \left[1 - \frac{q}{0.23\sqrt{\Gamma_\circ}}\right] + \sqrt{p} - 1 = 0 \qquad (11)$$

where θ is in radians. After solving for $\Gamma_\circ$ using an iterative technique, we can calculate the real part of the dielectric constant ϵ'_r from (5) by ignoring the imaginary part ϵ''_r, which is a valid approximation for a soil material. Next, the moisture content m_v and the imaginary part of the dielectric content ϵ''_r can be determined from the model given in [11]. Finally, with $\Gamma_\circ$ known, the roughness parameter ks can be determined from (6).

Because the copolarized and cross-polarized ratios p and q are not sensitive to surface roughness for very rough surfaces ($ks > 3$), this technique cannot estimate ks for such surfaces. Hence, it is preferable to use radar observations at the lowest available frequency for estimating the moisture content and rms height of a bare soil surface. By way of illustrating the

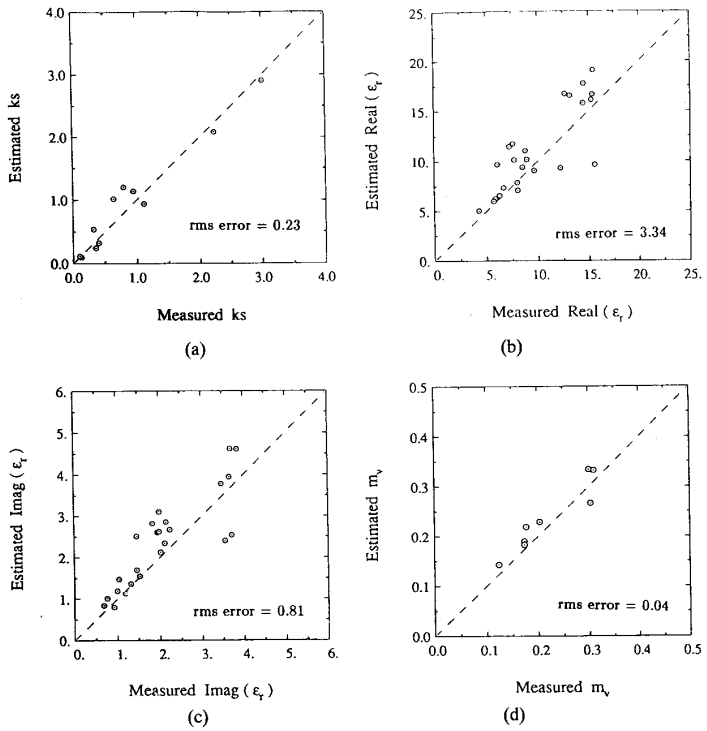

Fig. 17. Comparison between the values of surface parameters estimated by the inversion technique and those measured *in situ* for (a) ks, (b) the real part of ϵ_r, (c) the imaginary part of ϵ_r, and (d) the volumetric moisture content m_v.

capability of the inversion technique, we present in Fig. 17(a) the values of *ks* estimated by the inversion technique plotted against the values measured *in situ*. The data points include the data measured in support of this study for all surface conditions, but exclude surfaces for which $ks > 3$. of Figs. 17(b) and (c) show the results for ϵ_r' and ϵ_r'', respectively, for all surfaces measured in this study (the inversion technique is capable of estimating $\epsilon_r', \epsilon_r''$, and m_v for any ks, but it is incapable of estimating ks if $ks > 3$), and Fig. 17(d) presents the results for m_v. Note that for each value of m_v, we have three sets of values for $\epsilon_r', \epsilon_r''$, and ks, corresponding to the three frequencies used in this study.

The results displayed in Fig. 17 represent the first demonstration ever reported of a practical algorithm for estimating the roughness, dielectric constant, and moisture content of a bare soil surface from multipolarized radar observations. Before this technique can be widely applied, however, it is prudent to conduct additional experiments over a wide range of roughness and moisture conditions.

VI. Concluding Remarks

The major results of this study are summarized as follows:

1) At microwave frequencies, the available rough-surface scattering models are incapable of predicting the scattering behavior observed for bare-soil surface.
2) The copolarized ratio $p = \sigma^\circ_{hh}/\sigma^\circ_{vv} \leq 1$ for all angles, roughness conditions, and moisture contents; p increases rapidly with increasing ks up to $ks \simeq 1$, then it increases at a slower rate, reaching the value 1 for $ks > 3$. For $ks < 3$, p decreases with increasing incidence angle and with increasing moisture content.
3) The cross-polarized ratios $q = \sigma^\circ_{hv}/\sigma^\circ_{vv}$ exhibits a strong dependence on ks and a relatively weak dependence on moisture content. The ratio q increases rapidly with increasing ks up to $ks \simeq 1$, then it increases at a slower rate, reaching a constant value (that depends on the moisture content) for $ks > 3$.
4) The proposed scattering model provides very good agreement with experimental observations made over the ranges $0.1 \leq ks \leq 6, 2.5 \leq kl \leq 20$, and $0.09 \leq m_v \leq 0.31$. The model was found to be equally applicable when tested against radar data measured for surfaces with parameters outside the above ranges.
5) Soil moisture content (m_v) and surface roughness (ks) can be retrieved from multipolarized radar observations by applying the inversion technique developed in this paper.

References

[1] S. O. Rice, "Reflection of electromagnetic waves by slightly rough surfaces," *Commun. Pure Appl Math.*, vol. 4, pp. 351–378, 1951.
[2] L. Tsang, J. A. Kong, and R. T. Shin, *Theory of Microwave Remote Sensing*. New York: John Wiley and Sons, 1985.
[3] D. Wineberner and A. Ishimaru, "Investigation of a surface field phase perturbation technique for scattering from rough surfaces," *Radio Sci.*, vol. 20, pp. 161–170, Mar. 1985.
[4] P. Beckmann and A. Spizzichino, *The Scattering of Electromagnetic Waves from Rough Surfaces*. Norwood, MA: Artech House, 1987.

[5] F. T. Ulaby, M. K. Moore, and A. K. Fung, *Microwave Remote Sensing, Active and Passive*, vols. 2 and 3. Norwood, MA: Artech House, 1986.
[6] A. K. Fung and H. J. Eom, "Multiple scattering and depolarization by a randomly rough Kirchoff surface," *IEEE Trans. Antennas Propagat.*, vol. AP-26, pp. 463–471, May 1981.
[7] G. S. Brown, "Backscattering from a Gaussian distributed perfectly conducting rough surface," *IEEE Trans. Antennas Propagat.*, vol. AP-26, pp. 472–482, May 1978.
[8] M. A. Tassoudji, , K. Sarabandi, and F. T. Ulaby, "Design consideration and implementation of the LCX polarimetric scatterometer (POLARSCAT)," Rep. 022486–T-2, Radiation Laboratory, the University of Michigan, June 1989.
[9] K. Sarabandi and F. T. Ulaby, "A convenient technique for polarimetric calibration of radar systems," *IEEE Trans. Geosci. Remote Sensing*, vol. 28, pp. 1022–1033, 1990.
[10] D. R. Brunfeldt, "Theory and design of a field-portable dielectric measurement system," *IEEE Int. Geosci. Remote Sensing Symp. (IGARSS) Digest* vol. 1, pp 559–563, 1987.
[11] M. T. Hallikainen, F. T. Ulaby, M. C. Dobson, M. A. El-Rayes, and L. Wu, "Microwave dielectric behavior of wet soil -Part I: Empirical models and experimental observations," *IEEE Trans. Geosci. Remote Sensing*, vol. GE-23, pp 25–34, 1985.
[12] T. J. Jackson, "Laboratory evaluation of a field-portable dielectric/soil-moisture probe," *IEEE Trans. Geosci. Remote Sensing*, vol. 28, pp 241–245, Mar. 1990.
[13] H. Yamasaki, J. Awaka, A. Takahashi, K. Okamoto, and T. Ihara, "Measurements of soil backscatter with a 60 GHz scatterometer," *IEEE Int. Geosci. Remote Sensing Symp. (IGARSS '91) Digest*, vol. 2, pp 403–406, 1991.

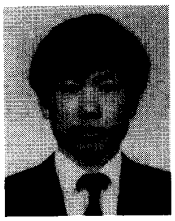

Yisok Oh (S'88) received the B.S. degree in electrical engineering from Yonsei University, Seoul, Korea, in 1982 and the M.S. degree in electrical engineering from the University of Missouri, Rolla, MO, in 1988.

He is currently working toward the Ph.D. degree at the University of Michigan, Ann Arbor, MI. His research interests include electromagnetic wave scattering from random surfaces and microwave remote sensing.

Kamal Sarabandi (S'87–M'90), for a photograph and biography, please see page 211 of this issue of the TRANSACTIONS.

Fawwaz T. Ulaby (M'68–SM'74–F'80), for a photograph and biography, please see page 211 of this issue of the TRANSACTIONS.